Materials Today Communications 24 (2020) 101339

Contents lists available at ScienceDirect

Materials Today Communications

journal homepage: www.elsevier.com/locate/mtcomm

# Metallic behavior in STO/LAO heterostructures with non-uniformly atomic interfaces

Rafael A.C. Amoresi[a,b,*], Leonélio Cichetto Jr.[b,c], Amanda F. Gouveia[d], Yormary N. Colmenares[e], Marcio D. Teodoro[c], Gilmar E. Marques[c], Elson Longo[d], Alexandre Z. Simões[a], Juan Andrés[b], Adenilson J. Chiquito[c], Maria A. Zaghete[f]

[a] Faculty of Engineering of Guaratinguetá, São Paulo State University, UNESP, 12516-410, Guaratinguetá, SP, Brazil
[b] Department of Analytical and Physical Chemistry, University Jaume I (UJI), Castello, 12071, Spain
[c] Department of Physics FederalUniversity of São Carlos, UFSCAR, 13565-905, São Carlos, SP, Brazil
[d] CDMF, Federal University of São Carlos, UFSCAR, 13565-905, São Carlos, SP, Brazil
[e] Institute of Physics of São Carlos, University of São Paulo – USP, 13560-970, São Carlos, Brazil
[f] Interdisciplinary Laboratory of Electrochemistry and Ceramics, LIEC, Chemistry Institute, São Paulo State University, UNESP, 14800-060, Araraquara, SP, Brazil

ARTICLE INFO

This article is dedicated to Professor Dr. Maria A. Zaghete, whose dedication, scientific criticality, and extensive work has resulted in the training of countless researchers and articles that have further developed Science.

*Keywords:*
$LaAlO_3/SrTiO_3$ interface
Two-dimensional electron gas (2DEG)
Thin film oxygen pressure
Electronic transport properties
DFT calculations

ABSTRACT

The search for new and low-power switching devices involving the integration of semiconductor thin films is of interest, and has led to renewed research because such devices may exhibit innovative properties. Here, we investigate the two-dimensional electron gas (2DEG) at the $LaAlO_3/SrTiO_3$ interface with metallic and insulator behavior. Insight is offered by quantifying the interface charge distribution associated with structural and electronic order-disorder effects. Variations in the electron conductivity were observed to be associated with different specific clustering arrangements of both Ti and Al cations of the co-exposed surfaces at the interface, i.e., structural and electronic connectivity among the undercoordinated $[TiO_5]$ and $[AlO_5]$ clusters. These results indicate facet control as a strategy for enhancing the electric and magnetic properties of a device via the quantum confinement of electrons.

## 1. Introduction

The large number of studies on materials with heterojunctions generated by the co-exposed surfaces of the $ABO_3$ perovskite structure reflects the considerable research interest in these compounds. Their unique physico-chemical behavior and stability make them particularly appealing for a variety of technological applications. In particular, confined materials involving an atomically thin two-dimensional electron gas (2DEG) of perovskite heterostructures with structural anisotropy, rich surface chemistry, and unique electronic structures, are technologically intriguing because they exhibit fascinating changes and unusual behavior vis-à-vis their corresponding free state counterparts [1–12].

Since the first report by Hwang and Ohtomo [13] on the 2DEG at the interface of two otherwise insulating metal oxides, $SrTiO_3$ (STO) and $LaAlO_3$ (LAO), the LAO/STO heterostructure has been studied extensively owing to novel phenomena that are associated with the confinement of correlated electrons at the interface [14–16]. Several studies have revealed the wide range of technological applications of the heterostructure, such as in electronic devices [17], superconductors [18], and spintronics [19]. Understanding the properties and stability of these materials is the key to maximizing the impact of materials engineering [14,20,21]. Therefore, the ability to control both the atomic structure and composition of these oxide layers formed by $ABO_3$-based materials, as well as their interfaces, is emerging as one of the major challenges in the development of electronic devices with a range of functional properties.

With the advent of state-of-the-art thin-film deposition techniques,

* Corresponding author at: Faculty of Engineering of Guaratinguetá, São Paulo State University, UNESP, 12516-410, Guaratinguetá, SP, Brazil.
*E-mail addresses:* rafaelciola@yahoo.com.br, rciola@uji.es (R.A.C. Amoresi), cichetto@gmail.com (L. Cichetto), amandafernandes.gouveia@gmail.com (A.F. Gouveia), yncolmenares@gmail.com (Y.N. Colmenares), mdaldin@gmail.com (M.D. Teodoro), gemarques@df.ufscar.br (G.E. Marques), elson.liec@gmail.com (E. Longo), alezipo@yahoo.com (A.Z. Simões), andres@qfa.uji.es (J. Andrés), Chiquito@df.ufscar.br (A.J. Chiquito), maria.zaghete@unesp.br (M.A. Zaghete).

https://doi.org/10.1016/j.mtcomm.2020.101339
Received 27 May 2020; Accepted 5 June 2020
Available online 16 June 2020

such as pulsed laser deposition (PLD), atomically sharp interfaces can be manufactured [22–25]. Since oxidizing or reducing conditions can change the properties of the 2DEG, it is important to verify the actual impact under real operating conditions; then, the effect of the presence of oxygen can be investigated. It is also important to understand this phenomenon at a more fundamental level. Therefore, we set up the basis for further analysis of the experimental results with a theoretical picture of the electron system for the 2DEG at the LAO/STO interface. Ultimately, it is necessary to clarify these open questions not only because of their academic value, but also because of their key roles in understanding other systems that might show similar behaviors and how they could be utilized. Consequently, we revisited the origin of the 2DEG and further explored new ways of tuning its properties, based on a detailed density functional theory (DFT) study. Our results are expected to provide new knowledge about this type of interface system.

The main objective of the present work is to show that the electrical conductivity phenomena of interface are related to the interaction of arrangement of atomic clusters. Considering the constraints imposed by the two-dimensional conduction nature for the existence of the gas and the electron-electron correlation, we will investigate the properties of the metallic interface on the LAO/STO based on two carefully designed systems, oxygenated and non- oxygenated systems. LAO/STO films were obtained using PLD, and the underlying physical and chemical reasons for the metallic observation are discussed based on results from X-ray photoelectron spectroscopy, photoluminescence (PL) emissions, and temperature-dependent (magneto) transport measurements. To complement and rationalize the experimental results, first-principles DFT calculations were employed to obtain information at the interface between the LAO/STO heterojunction. To this end, structural analysis of the electron transfer process and monitored Mullikan charges calculations were performed to understand the structural and electronic order-disorder effects, providing new insight into the properties of this material. We complement these calculations with an investigation of the local coordination of La, Al, Sr, and Ti cations, i.e., the under-coordinated clusters on the surfaces.

The paper is organized as follows. In the next section, an overview is provided, in which the more relevant experimental and theoretical results in the literature are emphasized. In Section 3 the experimental methods are presented, comprising three subsections: the growth process of the LAO/STO interface, characterization techniques, and electrical and magnetic measurements. Our results are discussed in four separate subsections within Section 4: transport properties, structural and electronic order-disorder effects at the interface, and joint theoretical and experimental analysis of the formation process of the metallic interface. The main conclusions are summarized in Section 5.

## 2. Overview

The observation of a high charge mobility due to the presence of a 2DEG at the LAO/STO heterostructure has attracted widespread interest and motivated many studies that have attempted to find the origin and nature of the conductivity at the interface [26–28]. In addition, many other physical properties, not found in their bulk counterparts, have also been observed [17,18,29–35]. At the interface between of the LAO/STO heterostructure, a 2DEG of high mobility ($10^3$ $cm^2V^{-1}$ $s^{-1}$) [5,21] has been observed. Electrons move freely along an in-plane direction of the heterostructure interface while they are confined within a few nanometers of out-of-plane direction from the interface [13]. Studies have shown that there are electric and magnetic moment interactions with the neighboring atomic layers between STO and LAO [6–8]. In addition, a 2DEG has been observed on interfaces involving STO with $ABO_3$/STO ($A$ = La, Pr, Nd and $B$ = Al, Ga) [36–39] and $LaFeO_3$ [40] as an ultrathin epitaxial film. The processes generated by the presence of the 2DEG at the LAO/STO heterostructure can be considered assignature of a particular behavior of these interfaces, involving electronic band alignment that controls electron transport, the mechanical strain that changes the local electronic structure, and chemical bonding with the concomitant formation of new electronic states as active centers for trapping electrons and/or ions [41–44]. However, there is a lack of consensus regarding the nature and formation of the 2DEG, as different scenarios have been employed to rationalize this phenomena based on three main aspects: oxygen vacancies; structural deformation involving cation disorder; and electronic and orbital interface reconstruction [45–49].

DFT calculations using explicit atomistic models of the interface, have been extensively made for understanding the geometry and electronic properties of the LAO/STO interface. In this case, a polarity mismatch occurs at a polar–nonpolar interface of two oxide insulators, LAO and STO, and such an electrostatic discontinuity can drive an electronic/atomic reconstruction [50]. In real material systems, non-stoichiometry can coexist with polarity mismatch, but how they interact with each other and affect the electronic and magnetic properties is still unclear [26,51,52]. Therefore, an understanding of the interaction between non-stoichiometry and polar mismatch at the atomic level is necessary [53,54]. Usually, the nature of a semiconductor heterojunction is analyzed by looking at the band edges of the separate and interacting fragments, and the localization of holes and electrons in the interface associated with the process of charge carrier separation [55]. A plethora of simulations of LAO thin film on an STO substrate with *vacuum* on top of LAO have been performed to explain the conductivity associated with the formation of 2DEG at the LAO/STO and related interfaces [49,56–73].

The simulations are based on the construction of computational models with different interface combinations $(LaO)^+ - (SrO)^0$, $(LaO)^+ - (TiO_2)^0$, $(AlO_2)^- - (TiO_2)^0$, or $(AlO_2)^- - (SrO)^0$ surface termination. Recently, Guan et al. [74], studied the different models of LAO/STO heterostructures with a focus on the electronic properties of the interfaces and the influence of the geometry of the models on theoretical results. These simulations, based on the results of theoretical high-throughput methods, are capable of providing a direct comparison between experimental data and theoretical results. Furthermore, they provide a deeper insight, at the atomic level, that can be used to further determine the mechanism of 2DEG conductivity from the perspective of first-principles calculations. The identification of appropriate combinations of materials, explorations of new mechanisms, and then the practical realization of these interfaces should result in new technological applications.

To explain the origin of the 2DEG behavior, different mechanisms have been invoked based on the LaO/$TiO_2$-terminated (001) interface that are related to the polar $(LaO)^+$ and neutral $(TiO_2)^\circ$ planes joined at the interface [12,13,29]. They include the following: (i) a polar catastrophe mechanism in which the charge transfer process takes place from the polar $LaAlO_3$ to the nonpolar $SrTiO_3$ layers at the interface [27]; (ii) an oxygen vacancy-induced mechanism in the STO or LAO layers [45,75–78]; (iii) interdiffusion of interfacial cations to form an La/Sr interfacial mixing [46,79–82]; (iv) a mechanism related to the defect-free electronic reconstruction mechanism, in which Ti mixed valence states appear at the $(LaO)^+/(TiO_2)^\circ$ termination [47]; and (v) a mechanism related to charge-compensating defects formed by cationic vacancies [83]. However, it is increasingly evident that other LaO/$TiO_2$-terminated interfaces, terminated along the (110) and (111) surfaces instead of the (001) surface of LAO/STO interfaces, although having different polar natures, have similar conducting interfaces [48,84]. Recent studies reveal that non-uniform atomic terminations between $(AlO_2)^-/(SrO)^\circ$ atomic planes also presented conducting mechanisms [14]. This is related to the fact that the growth of the atomic layers is not based on a perfect long-range stoichiometry of the ions at the interface [21,79,80,85,86]. Furthermore, calculations show that the $AlO_2$ layer plays an important participation at the interface [58,87,88], which together with its thermodynamic surface instability compared to LaO [89,90], marks it as an important part of the STO/LAO interface. These results pave the way to a new line of research, as they indicate

that the interfacial atomic arrangement in LAO/STO interfaces is paramount, particularly in cases where the subsequent electronic properties of the material exhibit geometrical preferences along polar and/or crystallographic directions that feature inevitably complex surface reconstructions. Therefore, the nature of the mechanism of the interfacial conduction is still an open question and remains a key puzzle for these interfaces [91–93]. These findings prompt careful studies of the initial surfaces of perovskite film growth to correlate the physical behavior of the film with its interfacial structure.

## 3. Experimental section

### 3.1. Growth process of the LAO/STO heterojunction

For the deposition of the heterojunction, crystalline substrates of $SrTiO_3$ along the [100] direction were used. Surface treatments were performed on the substrates, based on the work of Koster et al. [94], for $TiO_2$ termination layers, and atomically flat $SrTiO_3$ surface was obtained, as confirmed by atomic force microscopy (Fig. S1a). $LaAlO_3$ films were grown by the PLD method in an ultra-high *vacuum* chamber using a KrF excimer laser with a wavelength of 248 nm. The frequency used was 2 Hz, and the laser beam was incident at 45° to the normal target surface at a fluence of 1.8 J/cm$^2$. The deposition temperature was 730 °C, and it was measured immediately on the back of the substrate fixed on the heater by a thermocouple. The base pressure was $10^{-9}$ mbar and the deposition pressure with continuous oxygen flow was $2 \times 10^{-4}$ mbar. The distance between the target and the substrate was 4 cm. After LAO growth, the sample set was then calcined for 60 min at an oxygen partial pressure of 200 mbar at 550 °C, and then cooled at the same $O_2$ pressure to room temperature; this sample set was named “oxygenated”. An additional set of samples was not oxygenated and cooled to room temperature at the same deposition oxygen pressure; these samples were named “non-oxygenated”. During the research, several samples were produced with thicknesses that varied between 3 and 40 nm. For samples with thicknesses between 15 and 40 nm, thickness measurements were performed using SEM in the cross section. Later the deposition rates were calculated and showed the expected behavior for thin films manufactured by PLD. [95,96] For the system of this work the deposition rate was calculated as 0.5 Å/shot, which is also expected for depositions using low pressures, as is our case, and with less than 800 shots. In this way the thickness of such a film was calculated to be approximately ~5.1 nm.

### 3.2. Characterization techniques

The surface were characterized by atomic force microscopy (AFM) (Digital Instruments, Model NanoScopeIIIa) using the tapping mode. Raman spectroscopy characterization was accomplished using aLabRAM iHR550 Horiba JobinYvon spectrometer with a 514-nm laser as the excitation source (spectral resolution of 1 cm$^{-1}$). X-ray diffraction (XRD) were performed with a diffractometer (Rigaku, Model Rint 2000). For surface characterization, X-ray photoelectron spectroscopy (XPS) measurements were obtained using a ScientaOmicron ESCA + spectrometer system equipped with a hemispherical analyzer (EA125) and a monochromatic source of Al Kα ($h\nu$ = 1486.7 eV). The source was rated at 280 W, while the spectrometer worked at a constant pass energy mode at 50 eV. All data analyses were made using CASA XPS Software (Casa Software Ltd., UK). The spectra were analyzed by first performing a Shirley background subtraction and correcting the charge effects using the C1s peak of adventitious carbon at 285.0 eV as a reference. Peak fitting was performed using an asymmetric Gaussian–Lorentzian product function (for the peak shape) and maintaining the ratio between spin-orbit splitting components. PL measurements were performed using a commercial confocal microscope (Attocube/CFMI) compatible with low temperatures and high magnetic fields. The samples were excited by a 355-nm laser coupled into a single-mode optical fiber, with the beam focused onto the sample by an aspheric lens. The luminescence was collimated by the same lens and projected into a 50-μm multimode optical fiber dispersed by a 75-cm spectrometer (Andor-Shamrock) and detected by a charged couple device (AndoriDus).

### 3.3. Electrical and magnetic measurements

For electrical and magnetic measurements, the devices were fabricated to enable analysis of the transport properties at the substrate/film interface. A conventional lithography process was used for defining the active regions (10 μm-wide Ti/Au alloy parallel bars) on the surface of the film. In the second step, a focused ion beam (FIB) microscope was used to drill the surface of the films so that it would make direct contact with the interface. The devices were drilled by an electron beam to reach the LAO/STO interface, and Pt was injected into the drilled holes in order contact with the 2DEG region according to a previous report [97]. Transport measurements were performed at different temperatures (8–300 K) using a closed-cycle He cryostat (Janis Research®, CCS150 model). The samples were maintained at a pressure lower than $5 \times 10-6$ mbar. The resistance was obtained using standard low frequency AC lock-in (13 Hz) and DC techniques, but the results remained unchanged. We used different current levels in the experiments to avoid non-linear transport due to high-field effects and undesired Joule heating. Initial electrical characterization (current-voltage curves) showed a linear shape as expected. We also conducted four- and two-probe measurements in different samples, but the resistivity/resistance also remained unchanged in the entire temperature range. Magnetoresistance measurements were performed using a four-wire configuration connected to a source meter (Keithley, 2400C model) and placed inside an ultra-low vibration cryostat (Attocube, modelAttodry 1000) operating at 4 K. Amagnetic field up to 9 T was applied using Faraday geometry (perpendicular to the sample surface).

## 4. Results and discussion

### 4.1. Transport properties

Temperature-dependent resistance curves R(T) of samples obtained are shown in Fig. 1a, b. Different regions of the samples were analyzed, as shown in inset of figure. Here, an AC current excitation (100 nA–1 μA) was applied to the outer electrodes, and the longitudinal resistance was measured between two inner potentiometric probes along the current direction. Data exhibit metallic behavior for oxygenated sample, Fig. 1a. It is observed from literature that the heterostructured samples are grown in different ways, in some works the films are cooled by oxidation process [18,98] and others use the same deposition pressure [13,17]. In this sense, the second sample set was tested without the oxidation stage while cooling (non-oxygenated sample), Fig. 1b.

The curves for electrodes A to D for this sample set exhibit two distinct slope regions, which were assigned to two distinct conduction mechanisms. The point of transition is ~125 K. Above this point a metallic character is observed [99] and below this point the resistance data show an insulating character. Then, the set of non-oxygenated samples shows metal-to-insulator transition (MIT) behavior. Published works by Kalabukov et al. [75,100] and Sato et al. [101] have shown that the chemical environment of the heterostructure is very sensitive to obtain metallic or insulator behavior. Magnetoresistance measurements (Fig. 1c) were made between electrodes A and D for the sample that showed only metallic characteristics (oxygenated). A significant range of magnetoresistance was observed at 4 K, and it decreased as the temperature increased; this implies a characteristic for the presence of 2DEG [102–104].

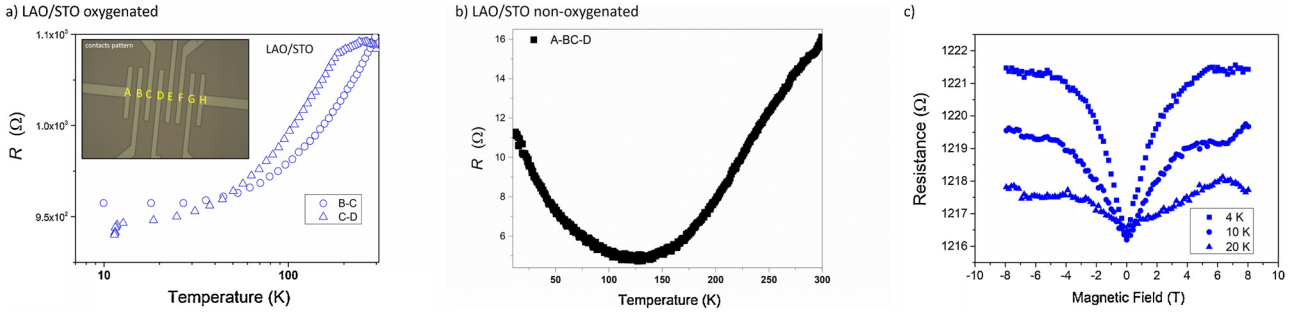


**Fig. 1.** Transport curves for the sample sets without and with the oxygenation step: measurements of the temperature dependent resistance for a) oxygenated and b) non-oxygenated films (inset: the contact patterns used); c) Magnetoresistance curves in which a magnetic field is applied at ± 8 T at 4 K, 10 K, and 20 K at electrodes A through D of the oxygenated film.

### *4.2. Structural and electronic order-disorder effects at the interface*

In order to understand why the oxygenated and non-oxygenated samples show metallic and MIT behavior, respectively, morphological and structural analyses were performed. AFM measurements (Fig. S1) indicate lack of the typical terrace-step structure of the epitaxial film growth. Raman spectroscopy (Fig. S2a) and XRD analysis (Fig. S2b) were performed to investigate both short and long-range structural order, respectively. Raman spectroscopy, Fig. S2a, shows interface interactions between adjacent clusters which vary from previously reported in the literature. Fig. S2b shows the long-range analysis by XRD in which both systems - oxygenated and non-oxygenated–have peaks related to the cubic phase of the STO monocrystal, confirming the texturing of the films; however, to the non-oxygenated sample the presence of other peaks suggest the coexistence of secondary phases.

In order to analyze the surface composition of the samples, XPS analyses were performed. Comparing the quantitative results for atomic concentrations (Table 1), a significant difference is noted between the stoichiometry of the samples. The atomic concentration ratio Sr/Al or Ti/La is higher for oxygenated samples. It is suggested that the oxygenation of the system during the growth of the films increases the interdiffusion of the atoms of Sr and Ti in the heterostructure and consequently changes the chemical environment in the heterostructure [105]. In addition, the composition of Al appears higher for the oxygenated sample, which shows a metallic behavior only. This is different from the observed by Sato et al. [101] which demonstrates that the non-stoichiometry of the films results in a change in electrical conductivity, not observed in our samples. This difference is accompanied by a small shift of the Al 2p peak ($\Delta E = 0.36$ eV) in the oxygenated sample, shown by the high-resolution XPS spectra for both samples which are shown in Figs. 2 and 3, respectively.

The energy peaks associated with the upper part of the heterostructure, corresponding to the core levels Al 2*p* and La 3*d* of the LAO unit cells, are shown in Fig. 2. The binding energies for lanthanum and aluminum on the samples surface correspond to the reported results for $Al^{3+}$ and $La^{3+}$ oxidation states. These findings in intensity/position were already reported in the literature [85,106]. Qiao et al. [85] observed that, for the La 4*d* /Al 2*p* peak area ratios, equal intensities were obtained when comparing stoichiometric films with LAO single crystals. They reported that the difference in intensity is due to stoichiometric differences. Drera et al. [106] also observed a difference in the intensity of the La 4*d* peaks. They observed that samples presenting the highest peak intensity will be insulators, suggesting that the oxygen deposition pressure has a relevant effect on the cation stoichiometry during the formation of the film. We observed variations in both the shift of the 2*p* peaks and intensity of the La 3*d* peak (Fig. 3b). This may be attributed to a lower oxidation state [107], or alteration of the chemical environment related to the electron distribution around the ion.

Studying the effects of oxidation states, Palacio et al. [107] observed a minimum variation of 1.2 eV, whereas we have observed one of 0.3 eV (Al 2*p* peak), which also ruled out the possibility of a change in the oxidation state of Al. However, bond energy variation as a result of the chemical environment is perfectly plausible; the structure of the films has a complex oxide configuration, and there are different studies [108,109] showing that different coordination geometries can be achieved. The octahedral environments have smaller binding energies than the tetrahedral environments without any changes in oxidation state [108,110,111]. We believe that this observation is consistent with our study.

Titanium cations at the interface region of samples are detectable by XPS owing to the few LAO unit cells above them. Studies have shown [112,105] the existence of a$Ti^{3+}$ state that appears as a shoulder at lower energies on the line $2p_{3/2}$ next to the main peak of $Ti^{4+}$. The authors suggested that the $Ti^{3+}$ component is only present in the first monolayers near the interface [105,113], and that this oxidation state is associated with the occupation of 3*d* empty states of Ti [38]. These cations would diffuse into the interface and then cause the high charge mobility [112,114]. However, Chambers et al. [80] have shown that the charges of ions that diffuse at the interface (Ti/Al and Sr/La) are completely compensated for, resulting in an invariance of the Ti oxidation state. The Ti 2*p* core levels of both samples are shown in Fig. 3a and c. The non-oxygenated system, with MIT behavior, has a Ti bonding energy, $2p_{3/2}$, centered at 459.5 eV, while for the oxygenated system, it is shifted to 458.8 eV, a variation in the lower binding energy of −0.7 eV. Both values correspond to the +4 oxidation state of Ti. However, the lower binding energy for Ti in the sample with metallic behavior only indicates an increase in electron density [115].

The O 1*s* peak for the two systems shows different symmetries, Fig. 3b and d. The non-oxygenated system presents sharp and asymmetric peak shape while the oxygenated system exhibits a broad and symmetric peak shape. The O 1*s* level is adjusted with three components each assigned from the highest to lowest binding energy: i) organic

**Table 1**
Relative atomic composition of oxygenated and non-oxygenated samples.

| | | | | | Composition | | Interdiffusion | |
|---|---|---|---|---|---|---|---|---|
| Sample | Ti % ( ± 0.2) | Sr % ( ± 0.2) | La % ( ± 0.2) | Al % ( ± 0.2) | Ti/Sr | Al/La | Sr/Al | Ti/La |
| Non-oxygenated | 0.5 | 4.8 | 33.6 | 61.1 | 0.1 | 1.8 | 0.08 | 0.01 |
| Oxygenated | 1.2 | 10.4 | 24.3 | 64.0 | 0.1 | 2.6 | 0.16 | 0.05 |

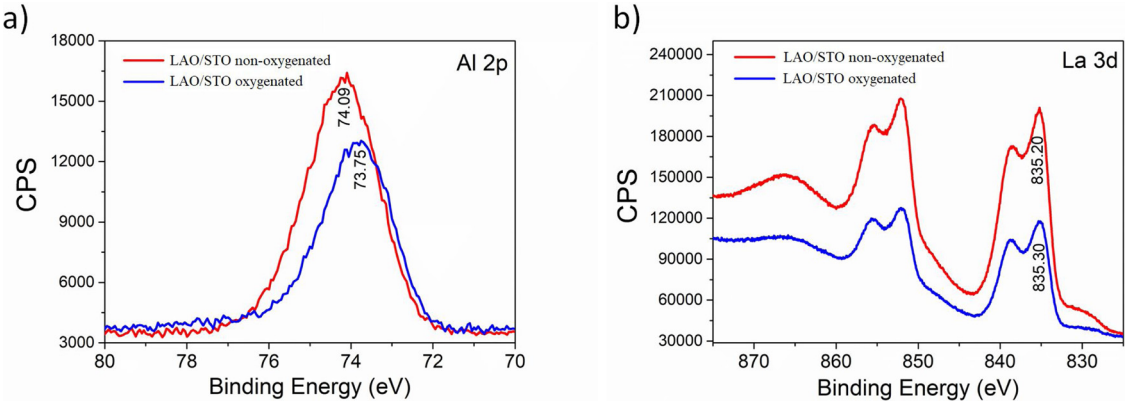


**Fig. 2.** XPS spectrum for a) Al 2p and b) La 3d collected from oxygenated and non-oxygenated systems. The spectra for Al 2p show a shift toward lower binding energy for the oxygenated system, and for the spectra of La 3d, a higher intensity for the non-oxygenated system compared to the oxygenated system.

groups C−$O_3$, $H_2O$ adsorbed, or $O_2$ adsorbed (~533 eV); ii) regions of oxygen deficiency compared to the matrix (~531 eV); and iii) the lattice oxygen (~530 eV) [116–120]. For the oxygenated system, the corresponding areas of the oxygen deficiency regions increase (49.14 %) in comparison to those of the non-oxygenated system (29.14 %). This region corresponds to a chemical environment with complex clusters disordered by the interatomic distance, bond angle, and dihedral angle that cause changes in the electronic density such that it is less localized than those of the dipoles. This effect is accentuated by the presence of oxygen vacancies in these clusters.

Therefore, considering the large number of defects in the structural environment, these can be related to the O 1*s* peak. At the same time, for the energy shift of lower binding energies for the Al 2*p* and Ti 3*d* peaks in the oxygenated system, it can be assumed that during the growth of films, at low oxygen pressures, there is a heavy contribution of tetrahedral clusters and that after oxygenation there is a large stabilization of the octahedral clusters (verified through an analysis of the energy of the cations' chemical environment) for Ti in the coordination of the films. It could be argued that the remaining defects of the structure correspond to both parts of the interface (Sr, Ti, / La/Al); however, for the oxygenated sample, the contribution of Ti and Sr is higher compared to the non-oxygenated sample. For this reason, the presence of different types of clusters of Ti, as the lattice former, should be considered at the interface region. This analysis leads us to believe that octahedral and tetrahedral clusters are present on the surface of the substrate during the LAO deposition. Enterkin et al. [121], when

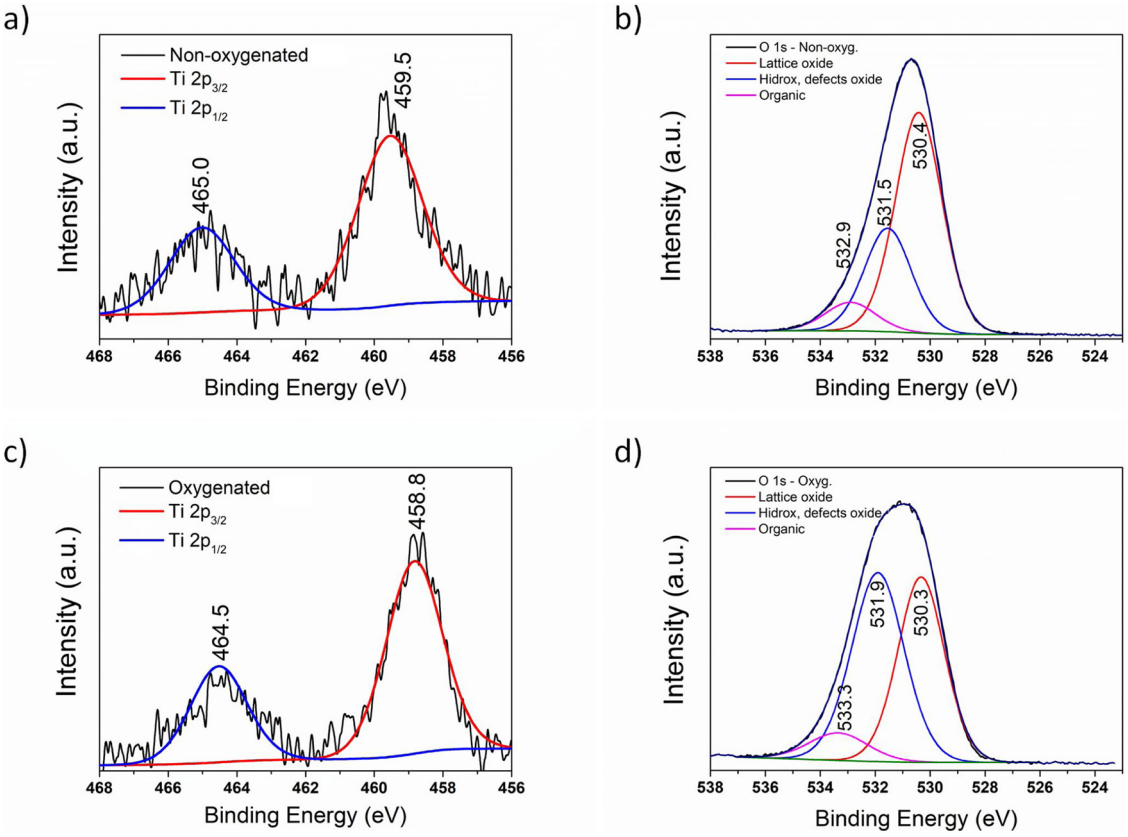


**Fig. 3.** XPS spectrum for (a, c) Ti 2p and (b, d) O 1s for the non-oxygenated and oxygenated system, respectively. The spectra show an oxidation state of +4 for Ti with variation for lower binding energy for the oxygenated system. The O1s spectra show an increase in the area corresponding to oxygen vacancies for the oxygenated system.

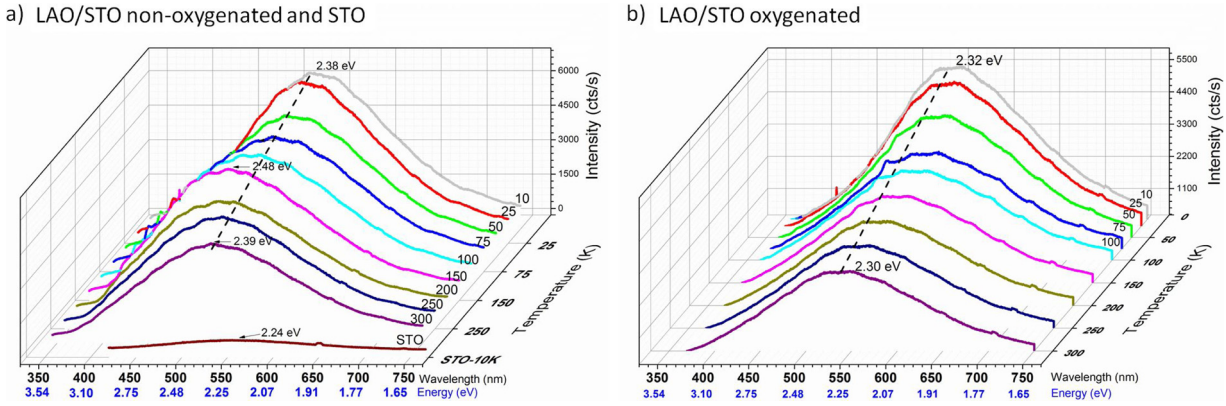


**Fig. 4.** Degree of order and disorder related to the PL spectra obtained in the temperature range of 10 to 300 K. In (a), for the pure STO substrate and for the non-oxygenated system, at 150 K, there is an emission displacement related to the disordered state. In (b), the spectra related to the oxygenated system.

studying the surface of STO, have also reported the possibility of the presence of these two types of clusters.

Accordingly, 2DEG formation process can be associated and explained by order–disorder degree of the materials. To this end, PL emissions in which their profile is a typical multiphonon process, were analyzed in the range from 10 to 300 K (Fig. 4) [122]. The two systems share similar PL characteristics. Both have high intensity emissions in the green region of 495–570 nm at low temperatures. The oxygenated system has a slightly shifted emission center at 2.32 eV (10 K) compared to the non-oxygenated system at 2.38 eV (10 K), $\Delta E = -60$ meV. PL emissions for the STO substrate show a low intensity signal. This is expected, as the PL emissions of oxides are generated by structural disorder [122,123], while the STO substrate is a single crystalline material. However, the intensity of the PL emissions of heterostructure samples is very intense owing to the presence of defect levels at the gap caused by order-disorder effects and oxygen vacancies [9,26,124,125]. For the non-oxygenated system the temperature variation induced changes in the PL spectrum.

There is a transition between 75–150 K, with a shift from 2.38 eV at 75 K to 2.48 eV at 150 K, $-\Delta E = 100$ meV, and a shift back to 2.39 eV at a higher temperature. The PL emissions in the present samples are related to the participation of several energy states, which are derived from the bulk, surface, and interface defects of both materials. The deconvolution of the PL emission spectra, Fig. S3, shows that at 150 K, for the non-oxygenated system, there is a shift of emission to higher energies with contributions of blue regions. For the oxygenated system changes in this region were not observed. This shift in the non-oxygenated system, sample with MIT behavior, can be energetically explained using oxygen vacancies of types $V_O^{\bullet}$ and $V_O^{\bullet\bullet}$, which are mono- and doubly-ionized types, respectively. As mono-ionized vacancies present at ~ 80 meV below the conduction band, and considering that the non-oxygenated system show $\Delta E = 100$ meV between 10–150 K (PL analysis), this is may represent this type of vacancy. Therefore, it is plausible to assume that the presence of these types of defects is significant to the charge transfer process at the oxide interface (2D gas), together with the scattering effects of the crystal lattice, and the strong electronic correlation in a perovskite structure [55].

### *4.3. Joint theoretical and experimental analysis of the metallic interface formation process*

The interface made by the co-exposed surfaces of $LaAlO_3/SrTiO_3$ was studied using an explicit atomistic model of the interface via density functional theory. The nature of the interface was evaluated by looking at the structure and considering the interfacial effects. The computational method, model systems, and technical details are given in the Supplementary Material. As previously mentioned, the theoretical results reveal that the type of termination and interface plays an important role in the interaction between the LAO and STO surfaces. When the interaction occurs at an interface composed of $(LaO)^{+} - (SrO)^{0}$ layers (Fig. S4a) or between the $(AlO_2)^{-} - (TiO_2)^{0}$ layers (Fig. S4c), an increase in the interatomic distance is observed. However, when there is an interaction between ($(LaO)^{+} - (TiO_2)^{0}$ or $(AlO_2)^{-} - (SrO)^{0}$) layers, a decrease in the interatomic distance occurs, resulting in a bond between the LAO and STO surface, as illustrated on Fig. S4b and d. To verify the model in which it is possible for free electrons to be present and the trapping of electrons to occur, the values of the Mulliken charge of each interface were calculated (Fig. S5) for the models where we observed an increase in the interatomic distance. The LAO/STO heterostructure formed by the $(LaO)^{+} - (SrO)^{0}$ interface exhibits a negative charge (Fig. S5a). This observation implies that there is a repulsive force between them, and the electrons can be repelled; consequently, an electron gas would not be formed. On the other hand, the LAO/STO heterostructure formed by the interaction on the $(AlO_2)^{-} - (TiO_2)^{0}$ interface (Fig. S5b) provides a perfect environment for trapping electrons between both materials, as the positive charge of the clusters attracts the electrons.

In the 2D interface composed of $(AlO_2)^{-} - (TiO_2)^{\circ}$, the three-dimensional chemical environment will be formed by clusters, i.e., under-coordinated $[TiO_5]$ and $[AlO_5]$ clusters, which are displayed in Fig. S4b. From these results, three more models were constructed to analyze the effect of excess O anions on the upper part of the heterostructure, simulating the experimental condition for the oxygenated system of the LAO/STO heterostructure. Fig. S6a shows the model represented in Fig. S4c with an excess of O atoms on the top of the LAO surface. The other two models are asymmetric (symmetric (asymmetric) model is when the bottom and top of the slab are with the same (different) termination of atoms) systems without excess oxygen (Fig. S6b) and with excess oxygen (Fig. S6c) on the top of LAO surface, which are related experimentally to the non-oxygenated and oxygenated system, respectively. The excess of O anions on top of the surfaces (Figs. S6a and c) are capable of eliminating the oxygen vacancies that are present in the $[AlO_5]$ and $[LaO_8]$ cluster; then, a complete local coordination, $[AlO_6]$ and $[LaO_{12}]$ cluster, are formed. The Mulliken charge of the clusters was also calculated and is shown in Fig. S6. From Fig. S6a, it is possible to affirm that the excess of O atoms in the $[TiO_5] - [AlO_5]$ model does not significantly affect the Mulliken charge of this clusters, despite an increase occurring in the interatomic distance between the STO and LAO (100) surfaces. Unlike in the non-stoichiometry symmetric model shown in Fig. S6a, in the case of the non-oxygenated stoichiometric model, Fig. S6b, with asymmetrical terminations, there is an increase in the Mulliken charge. This increase is a consequence of the structural and electronic disorder imposed by the stoichiometries that are capable of improving the capability of the environment to trap electrons on the interface of STO and LAO. For the oxygenated stoichiometry system, an increase in the values for the Mulliken charge of the clusters was also

observed.

These theoretical results reveal that, for metallic interface to be generated, the structure of STO and LAO on the (100) LAO/STO heterostructure needs to be formed by a stoichiometric system, as verified by the experimental relationship between Sr/Ti and the octahedral environment, and, as a consequence, by the asymmetrical terminations of the surface; furthermore, undercoordinated $[AlO_5]$ and $[TiO_5]$ clusters must be present on the interface. These asymmetrical terminations of the surface result in an increase in the disorder of the heterostructure, as also verified by the greater interdifussion of the metals in the sample with prominently metallic behavior. This hinders recombination and is also one of the reasons for the high electronic conductivity observed in heterostructured perovskite oxides.

From a thermodynamic point of view, the formation of defects can be explained by using energy criteria (cost to generate the defect) and entropy (how much is gained to generate the defect), as studied by Reinle-Schmitt et al. [126], who suggested that the 2DEG behavior originates from a stoichiometric layer between Sr/Ti and the insulating behavior of the LAO/STO interface is related to the presence of a layer rich in Sr. However, from our results we observed that the ratios of Ti/Sr for both systems, oxygenated and non-oxygenated, are the same, but that the defects present and the atomic interdiffusion are different in the two systems. This observation allows us to note that stoichiometry is not responsible for the metallic behavior; rather, it is the defects arising from the crystalline lattice former, Ti, which, according to *ab initio* calculations [127], predict a considerable increase in the charge density near the surface.

Therefore, the presence of Ti cations seems to be responsible for the electronic structure of surface defects. The local coordination of the Ti cation in the cubic structure corresponds to the $[TiO_6]$ clusters. However, by means of spectroscopic measurements [128,129], is demonstrated the lowest number of Ti−O coordination through $[TiO_5]$ clusters generated by the formation of oxygen vacancies ($V_O^x$). It is believed through the PL results ($\Delta E = 100$ meV) and studies already carried out by electron paramagnetic resonance spectroscopy [120,124], that shallow defects can exist, i.e., at a few meV below the conduction band of an intrinsic type, such as an oxygen vacancy, as a result of energy variation. To achieve this state, the system interface is processed as described below, eq. 01. Kröger-Vink notation was used, where the superscript ($x$) indicates a neutral charge, symbol (●) corresponds to a positive charge, and symbol ($'$) denotes a negative charge. The order and disorder clusters are represented by $[]_o$ and $[]_d$, respectively.

$$[TiO_6]_o^x + [TiO_5 \bullet V_O^x]_d \rightarrow [TiO_6]_d^{'} + [TiO_5 \bullet V_O^{\bullet}]_d \quad (1)$$

Therefore, from the results above and taking into account the interaction between the clusters, the chemical environment for the interface region, the degeneration of the orbitals from octahedral to tetrahedral $[TiO_4 \bullet 2V_O^x]_d$, the complexation of the aluminum clusters arranged in a tetrahedral or octahedral environment according to the oxygenation system, and the types of vacancies (mono or doubly ionized), the equations 02 to 06 can be exploited for the arrangement of defects around atomic clusters of interface regions:

$$[TiO_6]_o^x + [TiO_4 \bullet 2V_O^x]_d \rightarrow [TiO_6]_d^{'} + [TiO_4 \bullet V_O^x V_O^{\bullet}]_d \quad ((2))$$

$$[AlO_6]_d^{'} + [AlO_5 \bullet V_O^{\bullet}]_d \rightarrow [AlO_6]_o^x + [AlO_5 \bullet V_O^x]_d \quad ((3))$$

$$[AlO_5.\ V_o^x]_d + \frac{1}{2}O_2 \rightarrow [AlO_6]_o^{'} \quad ((4))$$

$$[TiO_4 \bullet 2V_O^x]_d + 2[AlO_6]_o^x \rightarrow [TiO_4 \bullet 2V_O^{\bullet}]_d + [AlO_6]_d^{'} \quad (5)$$

$$[TiO_4 \bullet 2V_O^x]_d \rightarrow [TiO_4 \bullet 2V_O^{\bullet\bullet}]_d + 4[AlO_6]_d^{'} \quad (6)$$

Our first-principles calculations demonstrate the accumulation of electrons at the bottom $n$-type and the top $p$-type $(AlO_2)^- - (TiO_2)^\circ$ interface. Therefore, to realize 2DEG practically, we focus on two issues: (1) building a p-type interface that consists of $AlO_2/TiO_2$ layers and (2) minimizing oxygen vacancies near the p-type interface, creating an adequate environment to trap electrons between both materials. Finally, we can also recover the orbital ordering of the mobile and localized electrons at oxygen-deficient LAO/STO interfaces, as it was employed, very recently, by Chikina et al. [49], to explain the formation and behavior of the 2DEG. In this interface, the octahedral crystal field with an oxygen vacancy, i.e., undercoordinated $[TiO_5]$ and $[AlO_5]$ clusters change the energy and occupancy of the $t_{2g}$ and $e_g$ states, and there is an exchange coupling process between the partially filled Ti$d_{xy}$ and half-filled Ti$e_g$ induced by the presence of oxygen vacancies at the interface [17,130–134].

## 5. Conclusions

In summary, we have investigated the 2DEG properties at the LAO/STO interface synthetized using pulsed laser deposition under both non-oxygenated and oxygenated conditions. This work we have highlighted the structural chemistry of the A- and B-sites of perovskite materials, STO and LAO, with computational work indicating the possibility of tuning the interface and surfaces so that they are suitable for 2DEG formation. Their structure and electronic properties have been studied by different experimental techniques and complemented by a first principles DFT calculation, using explicit atomistic models of the interface. The relation among the structure and electronic properties of the LAO/STO interface is rationalized by considering the relative contribution of three structural aspects: oxygen vacancies; structural deformations (including cation disorder); and electronic and orbital interface reconstruction. Our results reveal the importance of oxygen defects at the interface and surface of the LAO/STO. These defects are directly related to the partial pressure of oxygen during the preparation of the sample. Both experimental and theoretical results were employed to support our hypothesis, in which we propose the presence of undercoordinated $[TiO_5]$ and $[AlO_5]$ clusters of the co-exposed surfaces at the interface as key ingredient for metallic interface. Our study introduces the possibility of defect engineering through the manipulation of oxygen vacancies and facet control at the interface and surface of materials, which can be ultimately be helpful in understanding the formation mechanisms of 2DEG at metal oxide interfaces. We expect this new understanding will open up potential applications in future devices.

## CRediT authorship contribution statement

**Rafael A.C. Amoresi:** Conceptualization, Investigation, Methodology, Data curation, Writing - original draft. **Leonélio Cichetto:** Methodology, Investigation, Data curation. **Amanda F. Gouveia:** Software, Writing - original draft. **Yormary N. Colmenares:** Data curation, Writing - original draft. **Marcio D. Teodoro:** Investigation. **Gilmar E. Marques:** Funding acquisition. **Elson Longo:** Visualization, Funding acquisition. **Alexandre Z. Simões:** Investigation. **Juan Andres:** Writing - review & editing. **Adenilson J. Chiquito:** Investigation, Formal analysis, Validation, Writing - review & editing. **Maria A. Zaghete:** Conceptualization, Investigation, Supervision.

## Declaration of Competing Interest

The authors declare that they have no known competing financial interests or personal relationships that could have appeared to influence the work reported in this paper.

## Acknowledgements

The authors acknowledge the CEPID/CDMF and the São Paulo

Research Foundation (FAPESP) (Prof. Nos. 2013/07296-2, 2014/01371-5, 2017/23663-6, 2018/01914-0, 2019/09296-6 and 2017/19143-7), National Council for Scientific and Technological Development (CNPq) (No 150949/2018-9), and the Coordenação de Aperfeiçoamento de Pessoal de Nível Superior (CAPES) for the financial support granted in the course of this research. We are also grateful to the LMA-IQ for providing the FEG-FIB-SEM facilities. The Brazilian authors acknowledge the financial support of the following Brazilian research financing institutions: CNPq (150949/2018-9), FAPESP (2013/07296-2, 2017/19143-7, 2018/01914-0 and 2019/09296-6), and CAPES. J.A. acknowledges the financial support from the Generalitat Valenciana for Prometeo II/2014/022, ACOMP/2015/1202, the Spanish Ministerio de Economia y Competitividad (MINECO), project CTQ2015-65207-P, Ministerio de Ciencia, Innovación y Universidades (Spain) project PGC2018-094417-B-I00 and Universitat Jaume I, project no. UJI-B2016-25. To Emily Mary Grandoli, native English speaker, for reviewing the translation of this text.

## Appendix A. Supplementary data

Supplementary material related to this article can be found, in the online version, at doi:https://doi.org/10.1016/j.mtcomm.2020.101339.

## References

[1] S. Thiel, G. Hammerl, A. Schmehl, C.W. Schneider, J. Mannhart, Tunable quasi-two-dimensional electron gases in oxide heterostructures, Science (80-.) 313 (2006) 1942–1945, https://doi.org/10.1126/science.1131091.

[2] A. Ohtomo, D.A. Muller, J.L. Grazul, H.Y. Hwang, Artificial charge-modulationin atomic-scale perovskite titanate superlattices, Nature 419 (2002) 378–380, https://doi.org/10.1038/nature00977.

[3] M. Huijben, G. Koster, M.K. Kruize, S. Wenderich, J. Verbeeck, S. Bals, E. Slooten, B. Shi, H.Ja. Molegraaf, J.E. Kleibeuker, S. van Aert, J.B. Goedkoop, A. Brinkman, D.Ha. Blank, M.S. Golden, G. van Tendeloo, H. Hilgenkamp, G. Rijnders, Defect engineering in oxide heterostructures by enhanced oxygen surface exchange, Adv. Funct. Mater. 23 (2013) 5240–5248, https://doi.org/10.1002/adfm.201203355.

[4] H. Hilgenkamp, Novel transport phenomena at complex oxide interfaces, MRS Bull. 38 (2013) 1026–1031, https://doi.org/10.1557/mrs.2013.262.

[5] M. Ben Shalom, A. Ron, A. Palevski, Y. Dagan, Shubnikov-de Haas oscillations in SrTiO3/LaAlO3 interface, Phys. Rev. Lett. 105 (2010) 1–4, https://doi.org/10.1103/PhysRevLett.105.206401.

[6] P. Moetakef, C.A. Jackson, J. Hwang, L. Balents, S.J. Allen, S. Stemmer, Toward an artificial Mott insulator: correlations in confined high-density electron liquids in SrTiO3, Phys. Rev. B 86 (2012) 201102, , https://doi.org/10.1103/PhysRevB.86.201102.

[7] R. Ghosh, D. Basak, S. Fujihara, Effect of substrate-induced strain on the structural, electrical, and optical properties of polycrystalline ZnO thin films, J. Appl. Phys. 96 (2004) 2689, https://doi.org/10.1063/1.1769598.

[8] A. Aezami, M. Abolhassani, M. Elahi, Exchange interaction, electronic structure and magnetic properties of (LaMnO3)m/(SrTiO3)n superlattices: ab initio study, J. Alloys Compd. 587 (2014) 778–782, https://doi.org/10.1016/j.jallcom.2013.10.242.

[9] V.M. Longo, L.S. Cavalcante, M.G.S. Costa, M.L. Moreira, A.T. de Figueiredo, J. Andrés, J.A. Varela, E. Longo, First principles calculations on the origin of violet-blue and green light photoluminescence emission in SrZrO3 and SrTiO3 perovskites, Theor. Chem. Acc. 124 (2009) 385–394, https://doi.org/10.1007/s00214-009-0628-7.

[10] R.A.C. Amoresi, V. Teodoro, G.F. Teixeira, M.S. Li, A.Z. Simões, L.A. Perazolli, E. Longo, M.A. Zaghete, Electrosteric colloidal stabilization for obtaining SrTiO3/TiO2 heterojunction: microstructural evolution in the interface and photonics properties, J. Eur. Ceram. Soc. 38 (2018) 1621–1631, https://doi.org/10.1016/j.jeurceramsoc.2017.10.056.

[11] H. Guo, W.A. Saidi, J. Yang, J. Zhao, Nano-scale polar-nonpolar oxide heterostructures for photocatalysis, Nanoscale 8 (2016) 6057–6063, https://doi.org/10.1039/C5NR08689B.

[12] S. Thiel, G. Hammerl, A. Schmehl, C.W. Schneider, J. Mannhart, Tunable quasi-two-dimensional electron gases in oxide heterostructures, Science 313 (2006) 1942–1945, https://doi.org/10.1126/science.1131091.

[13] A. Ohtomo, H.Y. Hwang, A high-mobility electron gas at the LaAlO3/SrTiO3 heterointerface, Nature 427 (2004) 423–427.

[14] H. Lee, N. Campbell, J. Lee, T.J. Asel, T.R. Paudel, H. Zhou, J.W. Lee, B. Noesges, J. Seo, B. Park, L.J. Brillson, S.H. Oh, E.Y. Tsymbal, M.S. Rzchowski, C.B. Eom, Direct observation of a two-dimensional hole gas at oxide interfaces, Nat. Mater. 17 (2018) 231–236, https://doi.org/10.1038/s41563-017-0002-4.

[15] A.K. Singh, T.C. Wu, M.C. Chen, M.Y. Song, W.L. Lee, C.P. Su, M.W. Chu, Influence of SrTiO3 capping layer on the charge transport at the interfaces of SrTiO3/LaAlO3/SrTiO3 (100) heterostructure, Phys. Rev. Mater. 2 (2018) 1–9, https://doi.org/10.1103/PhysRevMaterials.2.114009.

[16] D.V. Christensen, F. Trier, W. Niu, Y. Gan, Y. Zhang, T.S. Jespersen, Y. Chen, N. Pryds, Stimulating oxide heterostructures: a review on controlling SrTiO3-based heterointerfaces with external stimuli, Adv. Mater. Interfaces 6 (2019) 1–40, https://doi.org/10.1002/admi.201900772.

[17] A. Brinkman, M. Huijben, M. van Zalk, J. Huijben, U. Zeitler, J.C. Maan, W.G. van der Wiel, G. Rijnders, D.H. a Blank, H. Hilgenkamp, Magnetic effects at the interface between non-magnetic oxides, Nat. Mater. 6 (2007) 493–496, https://doi.org/10.1038/nmat1931.

[18] N. Reyren, S. Thiel, A.D. Caviglia, L.F. Kourkoutis, G. Hammerl, C. Richter, C.W. Schneider, T. Kopp, A.-S. Rüetschi, D. Jaccard, M. Gabay, D. a Muller, J.-M. Triscone, J. Mannhart, Superconducting interfaces between insulating oxides, Science 317 (2007) 1196–1199, https://doi.org/10.1126/science.1146006.

[19] E. Lesne, Y. Fu, S. Oyarzun, D.C. Vaz, H. Naganuma, G. Sicoli, M. Jamet, E. Jacquet, A. Fert, M. Bibes, L. Vila, Highly efficient and tunable spin-to-charge conversion through Rashba coupling at oxide interfaces, Nat. Mater. 15 (2016) 1261, https://doi.org/10.1038/NMAT4726.

[20] S. Stemmer, S.J. Allen, Two-dimensional electron gases at complex oxide interfaces, Annu. Rev. Mater. Res. 44 (2014) 151–171, https://doi.org/10.1146/annurev-matsci-070813-113552.

[21] M. Huijben, G. Koster, M.K. Kruize, S. Wenderich, J. Verbeeck, S. Bals, E. Slooten, B. Shi, H.J.A. Molegraaf, J.E. Kleibeuker, S. Van, J.B. Goedkoop, A. Brinkman, D.H.A. Blank, M.S. Golden, Defect engineering in oxide heterostructures by enhanced oxygen surface exchange, Adv. Funct. Mater. 23 (2013) 5240–5248, https://doi.org/10.1002/adfm.201203355.

[22] G. Li, W. Wang, W. Yang, H. Wang, Epitaxial growth of group III-nitride films by pulsed laser deposition and their use in the development of LED devices, Surf. Sci. Rep. 70 (2015) 380–423, https://doi.org/10.1016/j.surfrep.2015.06.001.

[23] H.M. Christen, G. Eres, Recent advances in pulsed-laser deposition of complex oxides, J. Phys. Condens. Matter 20 (2008) 264005, , https://doi.org/10.1088/0953-8984/20/26/264005.

[24] L. Cichetto Jr., S. Sergeenkov, J.C.C.A. Diaz, E. Longo, F.M. Araujo-Moreira, Influence of substrate on structural and transport properties of LaNiO3 thin films prepared by pulsed laser deposition, AIP Adv. 7 (2017), https://doi.org/10.1063/1.4971842.

[25] D.H.A. Blank, G.J.H.M. Rijnders, G. Koster, H. Rogalla, A new approach in layer-by-layer growth of oxide materials by pulsed laser deposition, J. Electroceram. 4 (2000) 311–318.

[26] Z.Q. Liu, C.J. Li, W.M. Lu, X.H. Huang, Z. Huang, S.W. Zeng, X.P. Qiu, L.S. Huang, A. Annadi, J.S. Chen, J.M.D. Coey, T. Venkatesan, Origin of the two-dimensional electron gas at LaAlO3/SrTiO3 interfaces: the role of oxygen vacancies and electronic reconstruction, Phys. Rev. X 3 (2013) 21010, https://doi.org/10.1103/PhysRevX.3.021010.

[27] P.R. Willmott, S.A. Pauli, R. Herger, C.M. Schlep??tz, D. Martoccia, B.D. Patterson, B. Delley, R. Clarke, D. Kumah, C. Cionca, Y. Yacoby, Structural basis for the conducting interface between LaAlO3 and SrTiO3, Phys. Rev. Lett. 99 (2007) 155502, , https://doi.org/10.1103/PhysRevLett.99.155502.

[28] J.E. Hamann-borrero, S. Macke, W.S. Choi, R. Sutarto, F. He, A. Radi, I. Elfimov, R.J. Green, M.W. Haverkort, V.B. Zabolotnyy, H.N. Lee, G.A. Sawatzky, V. Hinkov, Valence-state reflectometry of complex oxide heterointerfaces, Npj Quantum Mater. 1 (2016) 16013, https://doi.org/10.1038/npjquantmats.2016.13.

[29] H.Y. Hwang, Y. Iwasa, M. Kawasaki, B. Keimer, N. Nagaosa, Y. Tokura, Emergent phenomena at oxide interfaces, Nat. Publ. Gr. 11 (2012) 103–113, https://doi.org/10.1038/nmat3223.

[30] C. Richter, H. Boschker, W. Dietsche, R. Jany, F. Loder, L.F. Kourkoutis, D.A. Muller, J.R. Kirtley, C.W. Schneider, J. Mannhart, Interface superconductor with gap behaviour like a high-temperature superconductor, Nature 502 (2013) 528–531, https://doi.org/10.1038/nature12494.

[31] A.J. Millis, Moment of magnetism, Nat. Phys. 7 (2011) 749–750, https://doi.org/10.1038/nphys2087.

[32] S. Banerjee, O. Erten, M. Randeria, Ferromagnetic exchange, spin–orbit coupling and spiral magnetism at the LaAlO3/SrTiO3 interface, Nat. Phys. 9 (2013) 626–630, https://doi.org/10.1038/nphys2702.

[33] M. Salluzzo, S. Gariglio, D. Stornaiuolo, V. Sessi, S. Rusponi, C. Piamonteze, G.M. De Luca, M. Minola, Origin of interface magnetism in BiMnO3/SrTiO3 and LaAlO3/SrTiO3 heterostructures, Phys. Rev. Lett. 111 (2013), https://doi.org/10.1103/PhysRevLett.111.087204 087204_1-5.

[34] D.A. Dikin, M. Mehta, C.W. Bark, C.M. Folkman, C.B. Eom, V. Chandrasekhar, Coexistence of superconductivity and ferromagnetism in two dimensions, Phys. Rev. Lett. 107 (2011) 56802, https://doi.org/10.1103/PhysRevLett.107.056802.

[35] L. Li, C. Richter, J. Mannhart, R.C. Ashoori, Coexistence of magnetic order and two-dimensional superconductivity at LaAlO3/SrTiO3 interfaces, Nat. Phys. 7 (2011) 762–766, https://doi.org/10.1038/nphys2080.

[36] P. Perna, D. Maccariello, M. Radovic, I. Pallecchi, M. Codda, J. Gazquez, M. Varela, S.J. Pennycook, F.M. Granozio, Conducting interfaces between band insulating oxides: the LaGaO3/SrTiO3 heterostructure, Appl. Phys. Lett. 97 (2010) 152111.

[37] A. Annadi, A. Putra, Z.Q. Liu, X. Wang, K. Gopinadhan, Z. Huang, S. Dhar, T. Venkatesan, Ariando, Electronic correlation and strain effects at the interfaces between polar and nonpolar complex oxides, Phys. Rev. B - Condens. Matter Mater. Phys. 86 (2012) 1–5, https://doi.org/10.1103/PhysRevB.86.085450.

[38] U. Treske, N. Heming, M. Knupfer, B. Büchner, E. Di Gennaro, A. Khare, U. Scotti, D. Uccio, F.M. Granozio, S. Krause, A. Koitzsch, Universal electronic structure of polar oxide hetero-interfaces, Nat. Publ. Gr. 5 (2015) 14506, https://doi.org/10.1038/srep14506.

[39] C. Li, Z. Liu, W. Lu, X.R. Wang, A. Annadi, Z. Huang, S. Zeng, T. Venkatesan, Tailoring the two dimensional electron gas at polar ABO3/SrTiO3 interfaces for oxide electronics, Sci. Rep. 5 (2015) 13314, https://doi.org/10.1038/srep13314.

[40] P. Xu, W. Han, P.M. Rice, J. Jeong, M.G. Samant, K. Mohseni, H.L. Meyerheim, S. Ostanin, I.V. Maznichenko, I. Mertig, E.K.U. Gross, A. Ernst, S.S.P. Parkin, Reversible formation of 2D electron gas at the LaFeO3/SrTiO3 interface via control of oxygen vacancies, Adv. Mater. 29 (2017) 1604447, , https://doi.org/10.

1002/adma.201604447.
[41] Y. Pai, A. Tylan-tyler, P. Irvin, J. Levy, Physics of SrTiO3 -based heterostructures and nanostructures: a review, Rep. Prog. Phys. 81 (2018) 36503.
[42] H. Guo, W.A. Saidi, J. Zhao, Tunability of the two-dimensional electron gas at the LaAlO3/SrTiO3 interface by strain-induced ferroelectricity, Phys. Chem. Chem. Phys. 18 (2016) 28474–28484, https://doi.org/10.1039/c6cp04769f.
[43] F. Zhang, Y. Fang, N.Y. Chan, W.C. Lo, D.F. Li, Dynamic modulation of the transport properties of the LaAlO3/SrTiO3 interface using uniaxial strain, Phys. Rev. B 93 (2016) 214427.
[44] L. Wang, W. Pan, W.X. Hu, D.Y. Sun, Strain-induced indirect-to-direct bandgap transition in an np-type LaAlO3/SrTiO3(110) superlattice, Phys. Chem. Chem. Phys. 21 (2019) 7075–7082, https://doi.org/10.1039/C8CP07761D.
[45] N. Pavlenko, T. Kopp, E.Y. Tsymbal, J. Mannhart, G.A. Sawatzky, Oxygen vacancies at titanate interfaces: two-dimensional magnetism and orbital reconstruction, Phys. Rev. B 86 (2012) 64431, https://doi.org/10.1103/PhysRevB.86.064431.
[46] V. Vonk, J. Huijben, D. Kukuruznyak, A. Stierle, H. Hilgenkamp, A. Brinkman, S. Harkema, Polar-discontinuity-retaining A -site intermixing and vacancies at SrTiO3/LaAlO3 interfaces, Phys. Rev. B 85 (2012) 45401, https://doi.org/10.1103/PhysRevB.85.045401.
[47] R. Pentcheva, W.E. Pickett, Electronic phenomena at complex oxide interfaces: insights from first principles, J. Phys. Condens. Matter 22 (2010) 43001, https://doi.org/10.1088/0953-8984/22/4/043001.
[48] G. Herranz, F. Sanchez, N. Dix, M. Scigaj, J. Fontcuberta, High mobility conduction at (110) and (111) LaAlO3/SrTiO3 interfaces, Sci. Rep. 2 (2012) 758, https://doi.org/10.1038/srep00758.
[49] A. Chikina, F. Lechermann, M. Husanu, M. Caputo, C. Cancellieri, X. Wang, T. Schmitt, M. Radovic, V.N. Strocov, Orbital ordering of the mobile and localized electrons at oxygen-deficient LaAlO3/SrTiO3 interfaces, ACS Nano 12 (2018) 7927–7935, https://doi.org/10.1021/acsnano.8b02335.
[50] N. Nakagawa, H.Y. Hwang, D.A. Muller, Why some interfaces cannot be sharp, Nat. Mater. 5 (2006) 204–209, https://doi.org/10.1038/nmat1569.
[51] C.F. Chang, Z. Hu, S. Klein, X.H. Liu, R. Sutarto, A. Tanaka, J.C. Cezar, N.B. Brookes, H. Lin, H.H. Hsieh, C.T. Chen, A.D. Rata, L.H. Tjeng, Dynamic atomic reconstruction: how Fe3O4 thin films evade polar catastrophe for epitaxy, Phys. Rev. X 6 (2016) 41011, https://doi.org/10.1103/PhysRevX.6.041011.
[52] I. Tung, G. Luo, J.H. Lee, S.H. Chang, J. Moyer, H. Hong, M.J. Bedzyk, H. Zhou, D. Morgan, D.D. Fong, J.W. Freeland, Polarity-driven oxygen vacancy formation in ultrathin LaNiO3 films on SrTiO3, Phys. Rev. Mater. 1 (2017) 53404, https://doi.org/10.1103/PhysRevMaterials.1.053404.
[53] Y. Kim, A. Morozovska, E. Eliseev, M.P. Oxley, R. Mishra, S.M. Selbach, T. Grande, S.T. Pantelides, S.V. Kalinin, A.Y. Borisevich, Direct observation of ferroelectric field effect and vacancy-controlled screening at the BiFeO3/LaxSr1-xMnO3 interface, Nat. Mater. 13 (2014) 1019–1025, https://doi.org/10.1038/NMAT4058.
[54] F.Y. Bruno, M.N. Grisolia, C. Visani, S. Valencia, M. Varela, R. Abrudan, J. Tornos, S.J. Pennycook, Z. Sefrioui, C. Leon, J.E. Villegas, J. Santamaria, Insight into spin transport in oxide heterostructures from interface-resolved magnetic mapping, Nat. Commun. 6 (2015) 6306, https://doi.org/10.1038/ncomms7306.
[55] Y. Chen, R.J. Green, Progress and perspectives of atomically engineered perovskite oxide interfaces for electronics and electrocatalysts, Adv. Mater. Interfaces 1900547 (2019) 1–15, https://doi.org/10.1002/admi.201900547.
[56] F. Wang, J. Li, X. Zhang, J. Liu, M. Zhao, W. Su, C. Wang, L. Mei, Origin of the two-dimensional electron gas at the interface of NdGaO3/SrTiO3, Comput. Mater. Sci. 147 (2018) 87–94, https://doi.org/10.1016/j.commatsci.2018.01.030.
[57] H. Banerjee, S. Banerjee, M. Randeria, T. Saha-Dasgupta, Electronic structure of oxide interfaces: a comparative analysis of GdTiO3/SrTiO3 and LaAlO3/SrTiO3 interfaces, Sci. Rep. 5 (2016) 18647, https://doi.org/10.1038/srep18647.
[58] R. Pentcheva, W. Pickett, Avoiding the polarization catastrophe in LaAlO3 overlayers on SrTiO3(001) through polar distortion, Phys. Rev. Lett. 102 (2009) 107602, , https://doi.org/10.1103/PhysRevLett.102.107602.
[59] W. Son, E. Cho, J. Lee, S. Han, Hydrogen adsorption and carrier generation in LaAlO3 – SrTiO3 heterointerfaces: a first-principles study, J. Phys. Condens. Matter 22 (2010) 315501, , https://doi.org/10.1088/0953-8984/22/31/315501.
[60] A. Janotti, L. Bjaalie, L. Gordon, Controlling the density of the two-dimensional electron gas at the SrTiO3/LaAlO3 interface, Phys. Rev. B 86 (2012) 241108, , https://doi.org/10.1103/PhysRevB.86.241108.
[61] L. Zhang, X. Zhou, H. Wang, J. Xu, J. Li, E.G. Wang, S. Wei, Origin of insulating behavior of the p-type LaAlO3/SrTiO3 interface: polarization-induced asymmetric distribution of oxygen vacancies, Phys. Rev. B 82 (2010) 125412, , https://doi.org/10.1103/PhysRevB.82.125412.
[62] L. Weston, X.Y. Cui, S.P. Ringer, C. Stampfl, Density-functional prediction of a surface magnetic phase in SrTiO3/LaAlO3 heterostructures induced by Al vacancies, Phys. Rev. Lett. 113 (2014) 186401, , https://doi.org/10.1103/PhysRevLett.113.186401.
[63] H. Hu, L. Ao, A. Pham, D. Wang, Y. Wang, Z. Chen, C. Kong, T.T. Tan, X. Zu, S. Li, Oxygen vacancy dependence of magnetic behavior in the LaAlO3/SrTiO3 heterostructures, Adv. Mater. Interfaces 3 (2016) 1600547, , https://doi.org/10.1002/admi.201600547.
[64] J. Cheng, S. Nazir, K. Yang, First-principles prediction of two-dimensional electron gas driven by polarization discontinuity in nonpolar/nonpolar AHfO3/SrTiO3 (A = Ca, Sr, and Ba) heterostructures, ACS Appl. Mater. Interfaces 8 (2016) 31959–31967, https://doi.org/10.1021/acsami.6b06907.
[65] Y. Du, C. Wang, J. Li, X. Zhang, F. Wang, Y. Zhu, N. Yin, L. Mei, The effect of in-plane strain on the electronic properties of LaAlO3/SrTiO3 interface, Comput. Mater. Sci. 99 (2015) 57–61, https://doi.org/10.1016/j.commatsci.2014.11.039.
[66] A. Sorokine, D. Bocharov, S. Piskunov, V. Kashcheyevs, Electronic charge redistribution in LaAlO3 (001) thin films deposited at SrTiO3 (001) substrate: first-principles analysis and the role of stoichiometry, Phys. Rev. B 86 (2012) 155410, , https://doi.org/10.1103/PhysRevB.86.155410.
[67] D. Marton, J.W. Rabalais, Thermal stimulation of the surface termination of LaAlO3 {100}, J. Chem. Phys. 108 (1998) 1645–1652, https://doi.org/10.1063/1.475535.
[68] J. Li, W. Wu, Y. Shen, P. Zhang, Y. Hong, H. Bai, G. Li, From LaAlO3/SrTiO3 to LaAlO3/KNbO3: improving the transport properties of two-dimensional electronic gas in created +1/+1 interfaces, Comput. Theor. Chem. 156 (2019) 286–291, https://doi.org/10.1016/j.commatsci.2018.09.053.
[69] M. Behtash, S. Nazir, Y. Wang, K. Yang, Polarization effects on the interfacial conductivity in LaAlO3/SrTiO3 heterostructures: a first-principles study, Phys. Chem. Chem. Phys. 18 (2016) 6831–6838, https://doi.org/10.1039/c5cp07581e.
[70] J. Cho, H. Jeen, E. Cho, Density functional theory based interfacial studies of ABO3/SrTiO3 (A = La, Y, Sc, B = Al, Ga) and its relation to polar catastrophe, Thin Solid Films 651 (2018) 13–17, https://doi.org/10.1016/j.tsf.2018.02.001.
[71] S.J. Leake, S.A. Pauli, C. Cancellieri, D. Fontaine, S. Gariglio, N. Reyren, A.D. Caviglia, A. Fe, Electrostriction at the LaAlO3/SrTiO3 interface, Phys. Rev. Lett. 107 (2011) 56102, https://doi.org/10.1103/PhysRevLett.107.056102.
[72] Y.B. Xue, Y.Y. Shan, H. Xu, The role of boundary conditions in tuning the electronic properties of the (0 0 1) LaAlO3/SrTiO3 interface, Comput. Mater. Sci. 149 (2018) 354–359, https://doi.org/10.1016/j.commatsci.2018.03.044.
[73] I.V. Maznichenko, S. Ostanin, V.K. Dugaev, I. Mertig, A. Ernst, Impact of long-range disorder on the two-dimensional electron gas formation at a LaAlO3/SrTiO3 interface, Phys. Rev. Mater. 2 (2018) 74003, https://doi.org/10.1103/PhysRevMaterials.2.074003.
[74] L. Guan, F. Tan, G. Shen, Y. Liang, X. Xu, J. Guo, Applied Surface Science Comparison of geometry models in the study of perovskite heterostructures, Appl. Surf. Sci. 475 (2019) 185–190, https://doi.org/10.1016/j.apsusc.2018.11.248.
[75] A. Kalabukhov, R. Gunnarsson, J. Börjesson, E. Olsson, T. Claeson, D. Winkler, Effect of oxygen vacancies in the SrTiO3 substrate on the electrical properties of the LaAlO3/SrTiO3 interface, Phys. Rev. B - Condens. Matter Mater. Phys. 75 (2007), https://doi.org/10.1103/PhysRevB.75.121404 121404(R).
[76] M. Bibes, C. Carre, G. Herranz, M. Basletic, High mobility in LaAlO3/SrTiO3 heterostructures: origin, dimensionality, and perspectives, Phys. Rev. Lett. 98 (2007) 216803, , https://doi.org/10.1103/PhysRevLett.98.216803.
[77] W. Siemons, G. Koster, H. Yamamoto, W.A. Harrison, G. Lucovsky, T.H. Geballe, D.H.A. Blank, M.R. Beasley, Origin of charge density at LaAlO3 on SrTiO3 heterointerfaces: possibility of intrinsic doping, Phys. Rev. Lett. 98 (2007) 196802, , https://doi.org/10.1103/PhysRevLett.98.196802.
[78] C. Cen, S. Thiel, G. Hammerl, C.W. Schneider, K.E. Andersen, C.S. Hellberg, J. Mannhart, J. Levy, Nanoscale control of an interfacial metal-insulator transition at room temperature, Nat. Mater. 7 (2008) 298–302, https://doi.org/10.1038/nmat2136.
[79] L. Qiao, T.C. Droubay, T.C. Kaspar, P.V. Sushko, S.A. Chambers, Cation mixing, band offsets and electric fields at LaAlO3/SrTiO3 (001) heterojunctions with variable La:Al atom ratio, Surf. Sci. 605 (2011) 1381–1387, https://doi.org/10.1016/j.susc.2011.04.035.
[80] S.A. Chambers, M.H. Engelhard, V. Shutthanandan, Z. Zhu, T.C. Droubay, L. Qiao, P.V. Sushko, T. Feng, H.D. Lee, T. Gustafsson, E. Garfunkel, A.B. Shah, J.M. Zuo, Q.M. Ramasse, Instability, intermixing and electronic structure at the epitaxial LaAlO3/SrTiO3 (001) heterojunction, Surf. Sci. Rep. 65 (2010) 317–352, https://doi.org/10.1016/j.surfrep.2010.09.001.
[81] H. Zaid, M.H. Berger, D. Jalabert, M. Walls, R. Akrobetu, I. Fongkaew, W.R.L. Lambrecht, N.J. Goble, X.P.A. Gao, P. Berger, A. Sehirlioglu, Atomic-resolved depth profile of strain and cation intermixing around LaAlO3/SrTiO3 interfaces, Sci. Rep. 6 (2016) 28118, https://doi.org/10.1038/srep28118.
[82] Y.-L. Du, C.-J. Ji, X.-M. Zhang, C.-L. Li, X.-N. Fang, Tunable magnetic and half-metallic properties of the two-dimensional electron gas in LaAlO3/SrTiO3 (111) heterostructure, Phys. Chem. Chem. Phys. 21 (2019) 18170–18178, https://doi.org/10.1039/C9CP00746F.
[83] F. Gunkel, S. Wicklein, S. Hoffmann-Eifert, P. Meuffels, P. Brinks, M. Huijben, G. Rijnders, R. Waser, R. Dittmann, Transport limits in defect-engineered LaAlO3/SrTiO3 bilayers, Nanoscale 7 (2015) 1013–1022, https://doi.org/10.1039/C4NR06272H.
[84] E. Frantzeskakis, T. Chris, F. Fortuna, A.F. Santander-syro, 2D surprises at the surface of 3D materials: confined electron systems in transition metal oxides, J. Electron Spectros. Relat. Phenomena 219 (2017) 16–28, https://doi.org/10.1016/j.elspec.2016.10.001.
[85] L. Qiao, T.C. Droubay, T. Varga, M.E. Bowden, V. Shutthanandan, Z. Zhu, T.C. Kaspar, S.A. Chambers, Epitaxial growth, structure, and intermixing at the LaAlO3/SrTiO3 interface as the film stoichiometry is varied, Phys. Rev. B 83 (2011) 85408, https://doi.org/10.1103/PhysRevB.83.085408.
[86] Y. Segal, J.H. Ngai, J.W. Reiner, F.J. Walker, C.H. Ahn, X-ray photoemission studies of the metal-insulator transition in LaAlO3/SrTiO3 structures grown by molecular beam epitaxy, Phys. Rev. B 80 (2009) 241107, , https://doi.org/10.1103/PhysRevB.80.241107.
[87] R. Pentcheva, W.E. Pickett, Charge localization or itineracy at LaAlO3/SrTiO3 interfaces: hole polarons, oxygen vacancies, and mobile electrons, Phys. Rev. B 74 (2006) 35112, https://doi.org/10.1103/PhysRevB.74.035112.
[88] M.P. Warusawithana, C. Richter, J.A. Mundy, P. Roy, J. Ludwig, S. Paetel, T. Heeg, A.A. Pawlicki, L.F. Kourkoutis, M. Zheng, M. Lee, B. Mulcahy, W. Zander, Y. Zhu, J. Schubert, J.N. Eckstein, D.A. Muller, C.S. Hellberg, J. Mannhart, D.G. Schlom, LaAlO3 stoichiometry is key to electron liquid formation at LaAlO3/SrTiO3 interfaces, Nat. Commun. 4 (2013) 1–9, https://doi.org/10.1038/ncomms3351.
[89] J. Tang, J. Zhu, W. Qin, J. Xiong, Y. Zhang, Y. Li, Atomic relaxation and electronic redistribution of LaAlO3 (001) surfaces, Phys. Lett. A 365 (2007) 149–155, https://doi.org/10.1016/j.physleta.2006.12.072.
[90] J. Goniakowski, F. Finocchi, C. Noguera, Polarity of oxide surfaces and nanostructures, Rep. Prog. Phys. 71 (2008) 16501, https://doi.org/10.1088/0034-4885/71/1/016501.
[91] P. Xu, Y. Ayino, C. Cheng, V.S. Pribiag, R.B. Comes, P.V. Sushko, S.A. Chambers, B. Jalan, Predictive Control over Charge Density in the Two-Dimensional Electron Gas at the Polar-Nonpolar NdTiO3/SrTiO3 Interface, Phys. Rev. Lett. 117 (2016)

106803, , https://doi.org/10.1103/PhysRevLett.117.106803.
[92] C.W. Bark, D.A. Felker, Y. Wang, Y. Zhang, H.W. Jang, C.M. Folkman, J.W. Park, S.H. Baek, H. Zhou, D.D. Fong, Q. Pan, E.Y. Tsymbal, M.S. Rzchowski, C.B. Eom, Tailoring a two-dimensional electron gas at the LaAlO3/SrTiO3 (001) interface by epitaxial strain, Appl. Phys. Sci. 108 (2011) 4720–4724, https://doi.org/10.1073/pnas.1014849108.
[93] N.C. Bristowe, P. Ghosez, P.B. Littlewood, The origin of two-dimensional electron gases at oxide interfaces: insights from theory, J. Phys. Condens. Matter 26 (2014) 143201, , https://doi.org/10.1088/0953-8984/26/14/143201.
[94] G. Koster, B.L. Kropman, G.J.H.M. Rijnders, D.H.A. Blank, H. Rogalla, Quasi-ideal strontium titanate crystal surfaces through formation of strontium hydroxide, Appl. Phys. Lett. 73 (1998) 2920–2922.
[95] D. Dijkkamp, T. Venkatesan, X.D. Wu, S.A. Shaheen, N. Jisrawi, Y.H. Min-Lee, W.L. McLean, M. Croft, Preparation of Y-Ba-Cu oxide superconductor thin films using pulsed laser evaporation from high Tc bulk material, Appl. Phys. Lett. 51 (1987) 619–621, https://doi.org/10.1063/1.98366.
[96] R.E. Muenchausen, S.R. Foltyn, N.S. Nogar, R.C. Estler, E.J. Peterson, X.D. Wu, Laser-induced target modification effects on pulsed laser depositions of YBaCuO superconducting thin films, Nucl. Instruments Methods Phys. Res. Sect. A Accel. Spectrometers, Detect. Assoc. Equip. 303 (1991) 204–207, https://doi.org/10.1016/0168-9002(91)90789-S.
[97] R.A.C. Amoresi, L. Cichetto, S. Kundu, M.D. Teodoro, G.E. Marques, E. Longo, J. Andrés, A.J. Chiquito, M.A. Zaghete, S. Kundu, M.D. Teodoro, R.A.C. Amoresi, Direct preparation of standard functional interfaces in oxide heterostructures for 2DEG analysis through beam-induced platinum contacts, Appl. Phys. Lett. 113 (2018) 131603, , https://doi.org/10.1063/1.5046093.
[98] C.W. Schneider, S. Thiel, G. Hammerl, C. Richter, J. Mannhart, C.W. Schneider, S. Thiel, G. Hammerl, C. Richter, J. Mannhart, Microlithography of electron gases formed at interfaces in oxide heterostructures, Appl. Phys. Lett. 89 (2006) 122101, , https://doi.org/10.1063/1.2354422.
[99] A.J. Chiquito, A.J.C. Lanfredi, E.R. Leite, Electron-electron scattering in Sn doped In2O3 nanowires, Phys. E Low-Dimensional Syst. Nanostructures. 40 (2008) 449–451, https://doi.org/10.1016/j.physe.2007.06.059.
[100] A. Kalabukhov, Y.A. Boikov, I.T. Serenkov, V.I. Sakharov, J. Börjesson, N. Ljustina, E. Olsson, D. Winkler, T. Claeson, Improved cationic stoichiometry and insulating behavior at the interface of LaAlO3/SrTiO3 formed at high oxygen pressure during pulsed-laser deposition, Epl 93 (2011) 37001, https://doi.org/10.1209/0295-5075/93/37001.
[101] H.K. Sato, C. Bell, Y. Hikita, H.Y. Hwang, Stoichiometry control of the electronic properties of the LaAlO3/SrTiO3 heterointerface, Appl. Phys. Lett. 102 (2013) 251602, , https://doi.org/10.1063/1.4812353.
[102] X. Renshaw Wang, L. Sun, Z. Huang, W.M. Lü, M. Motapothula, A. Annadi, Z.Q. Liu, S.W. Zeng, T. Venkatesan, Ariando, Parallel charge sheets of electron liquid and gas in La0.5Sr0.5TiO3/SrTiO3 heterostructures, Sci. Rep. 5 (2016) 18282, https://doi.org/10.1038/srep18282.
[103] I.M. Lifshitz, G. Peshanski, Galvanomagnetic characteristics of metals with open fermi surfaces, Sov. Phys. JETP. 35 (1959) 875–883.
[104] A.A. Abrikosov, Galvanomagnetic phenomena in metals in the quantum limit, Sov. Phys. JETP. 29 (1969) 746–753 doi:1969JETP…29..746A..
[105] P.W. Lee, V.N. Singh, G.Y. Guo, H.-J. Liu, J.-C. Lin, Y.-H. Chu, C.H. Chen, M.-W. Chu, Hidden lattice instabilities as origin of the conductive interface between insulating LaAlO3 and SrTiO3, Nat. Commun. 7 (2016) 12773, https://doi.org/10.1038/ncomms12773.
[106] G. Drera, G. Salvinelli, A. Brinkman, M. Huijben, G. Koster, H. Hilgenkamp, G. Rijnders, D. Visentin, L. Sangaletti, Band offsets and density of Ti3+ states probed by X-ray photoemission on LaAlO3/SrTiO3 heterointerfaces and their LaAlO3 and SrTiO3 bulk precursors, Phys. Rev. B 87 (2013) 75435, https://doi.org/10.1103/PhysRevB.87.075435.
[107] C. Palacio, A. Arranz, Oxidation of iron deposited on polycrystalline aluminum surfaces, J. Phys. Chem. B 105 (2001) 10805–10811, https://doi.org/10.1021/jp010531p.
[108] a Mekki, D. Holland, K. Ziq, C.F. Mcconville, XPS and magnetization studies of cobalt sodium silicate glasses, J. Non Cryst. Solids 220 (1997) 267–279, https://doi.org/10.1016/S0022-3093(97)00300-1.
[109] Z. Zhou, Y. Zhang, Z. Wang, W. Wei, W. Tang, J. Shi, R. Xiong, Electronic structure studies of the spinel CoFe2O4 by X-ray photoelectron spectroscopy, Appl. Surf. Sci. 254 (2008) 6972–6975, https://doi.org/10.1016/j.apsusc.2008.05.067.
[110] J.J. Benitez, A. Diaz, Y. Laurent, J.A. Odriozola, Study of aluminophosphate oxynitride (AlPON) materials by X-ray photoelectron (XPS) and diffuse reflectance Fourier transform IR spectroscopy (DRIFTS), J. Mater. Chem. 8 (1998) 687–691.
[111] T.T.P. Cheung, K.W. Willcox, M.P. McDaniel, M.M. Johnson, The structure of coprecipitated aluminophosphate catalyst supports, J. Catal. 20 (1986) 10–20.
[112] M. Takizawa, S. Tsuda, T. Susaki, H.Y. Hwang, A. Fujimori, Electronic charges and electric potential at LaAlO 3/SrTiO 3 interfaces studied by core-level photoemission spectroscopy, Phys. Rev. B - Condens. Matter Mater. Phys. 84 (2011) 3–7, https://doi.org/10.1103/PhysRevB.84.245124.
[113] E. Slooten, Z. Zhong, H.J.A. Molegraaf, P.D. Eerkes, S. de Jong, F. Massee, E. van Heumen, M.K. Kruize, S. Wenderich, J.E. Kleibeuker, M. Gorgoi, H. Hilgenkamp, A. Brinkman, M. Huijben, G. Rijnders, D.H.A. Blank, G. Koster, P.J. Kelly, M.S. Golden, Hard x-ray photoemission and density functional theory study of the internal electric field in SrTiO3/LaAlO3 oxide heterostructures, Phys. Rev. B 87 (2013) 85128, https://doi.org/10.1103/PhysRevB.87.085128.
[114] A. Koitzsch, J. Ocker, M. Knupfer, M.C. Dekker, K. Dorr, B. Buchner, P. Hoffmann, In-gap electronic structure of LaAlO3-SrTiO3 heterointerfaces investigated by soft x-ray spectroscopy, Phys. Rev. B - Condens. Matter Mater. Phys. 84 (2011) 245121, , https://doi.org/10.1103/PhysRevB.84.245121.
[115] I.T. Chashechnikova, V.M. Vorotyntsev, V.V. Borovik, G.I. Golodets, I.V. Plyuto, A.P. Shpak, Strong metal-carrier interaction in cobalt- and nickel-titanium dioxide co-hydrogenation catalysts, Theor. Exp. Chem. 28 (1993) 176–178, https://doi.org/10.1007/BF00529413.
[116] B. Bharti, S. Kumar, H.-N. Lee, R. Kumar, Formation of oxygen vacancies and Ti3+ state in TiO2 thin film and enhanced optical properties by air plasma treatment, Sci. Rep. 6 (2016) 32355, https://doi.org/10.1038/srep32355.
[117] P.T. Hsieh, Y.C. Chen, K.S. Kao, C.M. Wang, Luminescence mechanism of ZnO thin film investigated by XPS measurement, Appl. Phys. A Mater. Sci. Process. 90 (2008) 317–321, https://doi.org/10.1007/s00339-007-4275-3.
[118] S. Sonsupap, P. Kidkhunthod, N. Chanlek, S. Pinitsoontorn, S. Maensiri, Fabrication, structure, and magnetic properties of electrospun Ce0.96Fe0.04O2 nanofibers, Appl. Surf. Sci. 380 (2016) 16–22, https://doi.org/10.1016/j.apsusc.2016.02.105.
[119] J. Miao, J. Sunarso, C. Su, W. Zhou, S. Wang, Z. Shao, SrCo1-xTixO3-$\delta$ perovskites as excellent catalysts for fast degradation of water contaminants in neutral and alkaline solutions, Sci. Rep. 7 (2017) 44215, https://doi.org/10.1038/srep44215.
[120] G. Zhang, W. Jiang, S. Hua, H. Zhao, L. Zhang, Z. Sun, Constructing bulk defective perovskite SrTiO3 nanocubes for high performance photocatalysts, Nanoscale 8 (2016) 16963–16968, https://doi.org/10.1039/C6NR04859E.
[121] J.A. Enterkin, A.K. Subramanian, B.C. Russell, M.R. Castell, K.R. Poeppelmeier, L.D. Marks, A homologous series of structures on the surface of SrTiO3(110), Nat. Mater. 9 (2010) 245–248, https://doi.org/10.1038/nmat2636.
[122] M.L. Moreira, M.F.C. Gurgel, G.P. Mambrini, E.R. Leite, P.S. Pizani, J.A. Yarda, E. Longo, Photoluminescence of barium titanate and barium zirconate in multilayer disordered thin films at room temperature, J. Phys. Chem. A 112 (2008) 8938–8942, https://doi.org/10.1021/jp801610y.
[123] L. Gracia, J. Andrés, V.M. Longo, J.A. Varela, E. Longo, A theoretical study on the photoluminescence of SrTiO3, Chem. Phys. Lett. 493 (2010) 141–146, https://doi.org/10.1016/j.cplett.2010.05.041.
[124] V.M. Longo, A.T. De Figueiredo, S. De Lázaro, M.F. Gurgel, M.G.S. Costa, C.O. Paiva-Santos, J.A. Varela, E. Longo, V.R. Mastelaro, F.S. De Vicente, A.C. Hernandes, R.W.A. Franco, Structural conditions that leads to photoluminescence emission in SrTiO3: an experimental and theoretical approach, J. Appl. Phys. 104 (2008) 23515, https://doi.org/10.1063/1.2956741.
[125] J.Q. Chen, X. Wang, Y.H. Lu, A. Roy Barman, G.J. You, G.C. Xing, T.C. Sum, S. Dhar, Y.P. Feng, Q.H. Xu, T. Venkatesan, Defect dynamics and spectral observation of twinning in single crystalline LaAlO3 under subbandgap excitation, Appl. Phys. Lett. 98 (2011) 41904, https://doi.org/10.1063/1.3543840.
[126] M.L. Reinle-Schmitt, C. Cancellieri, A. Cavallaro, G.F. Harrington, S.J. Leake, E. Pomjakushina, J.A. Kilner, P.R. Willmott, Chemistry and structure of homoepitaxial SrTiO3 films and their influence on oxide-heterostructure interfaces, Nanoscale 6 (2014) 2598, https://doi.org/10.1039/c3nr06456e.
[127] E. Heifets, R.I. Eglitis, E.A. Kotomin, J. Maier, G. Borstel, Ab initio modeling of surface structure for SrTiO3 perovskite crystals, Phys. Rev. B 64 (2001) 235417, , https://doi.org/10.1103/PhysRevB.64.235417.
[128] L.F. da Silva, W. Avansi, J. Andrés, C. Ribeiro, M.L. Moreira, E. Longo, V.R. Mastelaro, Long-range and short-range structures of cube-like shape SrTiO3 powders: microwave-assisted hydrothermal synthesis and photocatalytic activity, Phys. Chem. Chem. Phys. 15 (2013) 12386, https://doi.org/10.1039/c3cp50643f.
[129] F. Pontes, E. Longo, E. Leite, E.J. Lee, J. Varela, P. Pizani, C.E. Campos, F. Lanciotti, V. Mastellaro, C. Pinheiro, Photoluminescence at room temperature in amorphous SrTiO3 thin films obtained by chemical solution deposition, Mater. Chem. Phys. 77 (2002) 598–602, https://doi.org/10.1016/S0254-0584(02)00112-8.
[130] Ariando, X. Wang, G. Baskaran, Z.Q. Liu, J. Huijben, J.B. Yi, A. Annadi, A.R. Barman, A. Rusydi, S. Dhar, Y.P. Feng, J. Ding, H. Hilgenkamp, T. Venkatesan, Electronic phase separation at the LaAlO3/SrTiO3 interface, Nat. Commun. 2 (2011) 188, https://doi.org/10.1038/ncomms1192.
[131] Z. Salman, O. Ofer, M. Radovic, H. Hao, K.H. Chow, M.D. Hossain, C.D.P. Levy, W.A. Macfarlane, G.M. Morris, L. Patthey, M.R. Pearson, H. Saadaoui, T. Schmitt, D. Wang, R.F. Kiefl, Nature of weak magnetism in SrTiO3/LaAlO3 multilayers, Phys. Rev. Lett. 109 (2012) 257207.
[132] B. Kalisky, J.A. Bert, B.B. Klopfer, C. Bell, H.K. Sato, M. Hosoda, Y. Hikita, H.Y. Hwang, K.A. Moler, Critical thickness for ferromagnetism in LaAlO3/SrTiO3 heterostructures, Nat. Commun. 3 (2012) 922, https://doi.org/10.1038/ncomms1931.
[133] F. Lechermann, L. Boehnke, D. Grieger, C. Piefke, Electron correlation and magnetism at the LaAlO3/SrTiO3 interface: A DFT + DMFT investigation, Phys. Rev. B 90 (2014) 85125, https://doi.org/10.1103/PhysRevB.90.085125.
[134] M. Behrmann, F. Lechermann, Interface exchange processes in LaAlO3/SrTiO3 induced by oxygen vacancies, Phys. Rev. B 92 (2015) 125148, , https://doi.org/10.1103/PhysRevB.92.125148.